

# Viscoelastic effects on interfacial dynamics in air–liquid displacement under gravity stabilization

By ALEX G. LEE<sup>1</sup>†, ERIC S. G. SHAQFEH<sup>1,2</sup>‡  
AND BAMIN KHOMAMI<sup>3</sup>

<sup>1</sup>Department of Chemical Engineering, Stanford University, Stanford, CA 94305-5025, USA

<sup>2</sup>Department of Mechanical Engineering, Stanford University, Stanford, CA 94305-5025, USA

<sup>3</sup>Department of Chemical Engineering, Washington University, St Louis, MO 63130, USA

(Received 22 April 2003 and in revised form 26 October 2004)

We have investigated the role of liquid elasticity in the dynamics of air–liquid interfaces during immiscible fluid displacement flows. Our experimental studies of coating flows with gravity stabilization in an eccentric cylinder geometry for both a viscous Newtonian fluid and a series of elastic Boger fluids have uncovered two new elastically driven phenomena. First, elasticity is shown to create steady, two-dimensional ‘sharp interfaces’ under creeping flow conditions in forward-roll coating. Digital particle image velocimetry (DPIV) and DEVSS finite element techniques are applied to investigate the effect of gravity on both the flow field and the state of polymeric stresses near the free surface. Secondly, a new class of elastically driven stable substructures is shown to form and persist along the tip, i.e. the centre stagnation line, of the two-dimensional ‘sharp interfaces’ even after the onset of ribbing.

---

## 1. Introduction

Viscoelastic free surface flows have practical applications in coating technology, polymer processing, and enhanced oil recovery (Allen & Boger 1988; Poslinski, Oehler & Stokes 1995; Huzyak & Koelling 1997). A wide variety of coating geometries have been studied, including blade coaters, extrusion slot coaters, forward-roll coaters (co- and counter-rotating), and roll-plate coaters (Ruschak 1985). Numerous researchers in the past have focused on the coating of Newtonian fluids (in all the geometries mentioned above) in an effort to better understand and thereby prevent interfacial instabilities in industrial processes (Pearson 1959; Pitts & Greiller 1961; Mill & South 1967; Sullivan & Middleman 1979; Greener *et al.* 1980; Coyle, Macosko & Scriven 1990; Rabaud, Michalland & Couder 1990; Carvalho & Scriven 1999; Carvalho & Kheshgi 2000). Although most of the coating applications involve polymeric fluids, full-scale computational modelling of free surface flows of viscoelastic fluids has only been accomplished recently (Lee, Shaqfeh & Khomami 2002; Pasquali & Scriven 2002).

For Newtonian free surface flows in the surface-tension-dominated flow regime, the most important dimensionless parameter in analysing the flow dynamics is the

† Present address: Corporate Strategic Research, ExxonMobil Research & Engineering Co., P.O. BOX 998/1545 Rte. 22E., Annandale, NJ 08801-0998, USA.

‡ Author to whom correspondence should be addressed: eric@chemeng.stanford.edu

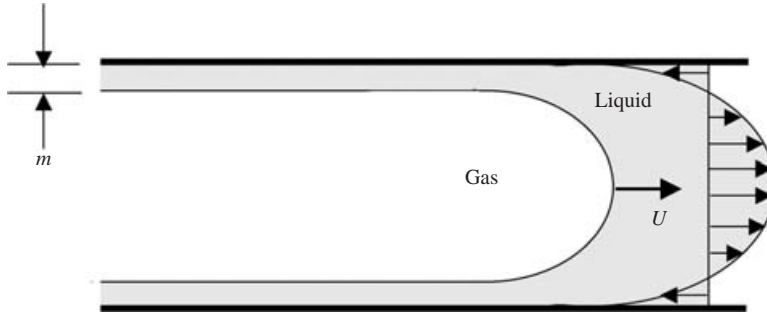


FIGURE 1. Gas-assisted displacement of a liquid in a channel or tube. The dimensionless film thickness,  $m$ , is defined in equation (3.1).

capillary number

$$Ca = \frac{\mu U}{\sigma} \quad (1.1)$$

where  $\mu$  is the viscosity of the liquid phase,  $\sigma$  the surface tension, and  $U$  the displacement velocity. The capillary number measures the relative importance of viscous and surface tension forces.

A widely studied interfacial flow is the displacement of a viscous liquid by an air bubble in a capillary tube (figure 1). Most of the literature on this flow can be traced back to the experiments conducted by Fairbrother & Stubbs (1935) and Taylor (1960), and the theoretical analysis pioneered by Bretherton (1961) for low-capillary-number Newtonian liquid displacements. Variations of the problem have since been analysed by various researchers both theoretically (Reinelt & Saffman 1985; Ruschak 1985; Lu & Chang 1988) and computationally (Giavedoni & Saita 1997; Lee *et al.* 2002). Early experimental studies on air-liquid displacement of non-Newtonian fluids were conducted by Bonn *et al.* (1995). Using solutions of poly(ethylene oxide) (PEO) and xanthane, they reported a film thickness increase over that found for Newtonian liquids in the plane flow geometry. Strong film thickening effects were also reported by Huzyak & Koelling (1997), who used highly elastic, non-shear-thinning, polyisobutylene/polybutene (PIB/PB) based Boger fluids in their capillary tube flow experiments. Ro & Homsy (1995) conducted the first theoretical study of free surface creeping flow created by the air displacement of a viscoelastic liquid initially filling a gap confined by two narrowly separated solid walls, i.e. the Hele-Shaw cell. The theory was formulated as a double perturbation expansion in powers of  $Ca^{1/3}$  and  $Wi/Ca^{1/3}$ , where  $Wi$  is the Weissenberg number. The Weissenberg number provides a measure of the elastic forces in the flow by introducing the relaxation time,  $\lambda$ , of the polymer as the second time scale in the problem

$$Wi = \frac{\lambda U}{b} \quad (1.2)$$

where  $b$  is the gap separation between the plates. Ro & Homsy concluded that for small  $Ca$  and  $Wi$  flows, the fluid elasticity induces resistance to streamwise straining and therefore reduces the coating film thickness. The apparent discrepancy between Ro & Homsy's theory and the experimental observations has been resolved in the finite element analysis conducted by Lee *et al.* (2002) where the onset of elastic stress boundary layers in the capillary-transition region of the air bubble at moderate values of  $Wi$  was shown to be the cause of film thickening in viscoelastic liquids.

Another classical problem on interfacial dynamics is the dip coating process, in which a thin liquid film is formed on a flat plate drawn at a certain angle from a liquid bath. The flux in withdrawal of a Newtonian liquid with dominant capillary forces was determined by Landau & Levich (1942) in their pioneering work. Other significant contributions have been made by White & Tallmadge (1965), who included gravity, and by Esmail & Hummel (1975), who considered fluid inertial effects. The corresponding problem for non-Newtonian liquids has been treated by Gutfinger & Tallmadge (1965), and by Spiers, Subbaraman & Wilkinson (1975). It is worth noting that inertial effects were not included in their theory, nor any non-Newtonian effect other than a shear-dependent viscosity. Using weakly elastic polyacrylamide/water liquids, Spiers *et al.* (1975) observed elasticity-driven film thinning in their experiments. The effect of elasticity on dip coating was first considered by Adachi, Spiers & Wilkinson (1978). They used a modified four-constant Oldroyd model coupled with an integral momentum balance approach to study the elasticity-driven film thickness variation. The agreement between their predictions and the experimental measurements by Spiers *et al.* was rather poor, however, and their numerical analysis failed to yield conclusive results.

Turning to the literature on the stability of interfacial flows, a comprehensive overview of the viscous fingering phenomena in Newtonian fluids in porous media and Hele-Shaw cell is described in an article by Homsy (1987). This class of instabilities is driven, in general, by differences in the pressure gradient between two fluids in fluid–fluid displacement flows. In the absence of gravity stabilization, if the displacing fluid is less viscous than the displaced fluid (which is the case for most coating flows), the interface may be unstable for all velocities. If the displacing fluid is more viscous then the interface is generally stable, though exceptions have been discovered recently (Michalland, Rabaud & Couder 1996; Chan 2000).

For immiscible Newtonian fluid displacement in a vertically positioned Hele-Shaw cell (less viscous upper fluid displacing a more viscous lower fluid), the gravity stabilization of the advancing interface will be significant if the distance between the parallel plates is large. The stability condition which determines the onset of fingering in the presence of gravity stabilization was obtained in an early analysis by Saffman & Taylor (1958). Their expression gives a critical condition for air  $\Rightarrow$  liquid displacement in terms of the dimensionless capillary number as

$$Ca_{crit} = \frac{\mu U}{\sigma} = \frac{(\rho - \rho_{air})gb^2}{12\sigma} \quad (1.3)$$

where  $\rho$  is the liquid density,  $\rho_{air}$  is the air density,  $g$  is the gravitational acceleration constant, and  $b$  is the gap width. Alternatively, we can write this condition as

$$\frac{Ca_{crit}}{Bo} = \frac{\mu U}{\Delta\rho gb^2} = Gr_{crit} = 1/12 \quad (1.4)$$

where the ratio of capillary number to Bond number is written as  $Gr$ , the gravity number. This dimensionless parameter measures the relative strength of the viscous forces and the gravity forces in the flow. For sufficiently small gaps, the gravity effects are small relative to surface tension (Coyle *et al.* 1990) since the associated Bond number,  $Bo = \Delta\rho gb^2/\sigma$ , is small.

Pearson (1959) and Pitts & Griller (1961) first examined the effects of flow channel geometry on the stability of Newtonian interfacial flows. They concluded that if the more viscous fluid was driven from a diverging channel, then the interface would be stable below a critical speed which was dependent on the divergence angle  $\alpha$  or wall slope  $\tan(\alpha/2)$ . Likewise displacement from a converging channel was

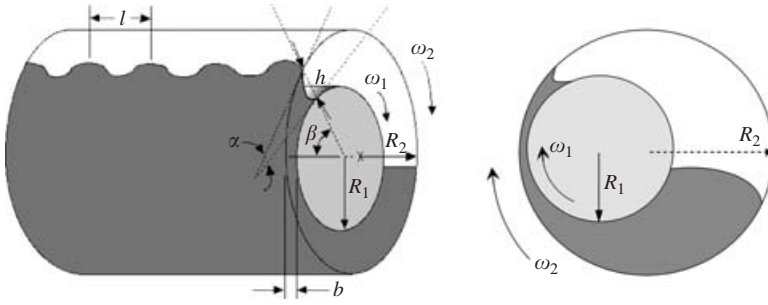


FIGURE 2. Eccentric-cylinder coating geometry.

destabilized relative to that between parallel walls. For a given diverging channel, Pitts & Greiller (1961) completed a one-dimensional stability analysis in the absence of gravity effects and found the critical condition to be:

$$Ca_{crit} = \frac{1}{3} \tan(\alpha/2). \quad (1.5)$$

Clearly, this result is only applicable for flows in the surface-tension-dominated regime (Ruschak 1985). Coyle *et al.* (1990) conducted a stability analysis on forward-roll coating versus the wall slope by using finite element simulations to model the two-dimensional free surface flow. Their stability analysis compared well with experimental data over two orders of magnitude of dimensionless gap widths.

The stability of polyacrylamide Boger fluids in the forward-roll coating and roll-plate geometries has been investigated by Bauman, Sullivan & Middleman (1982) and later by Dontula *et al.* (1996). Even for a liquid with a concentration of 10 p.p.m. of polymer which exhibited no measurable normal forces under shear, the critical conditions for the onset of ribbing decreased by a factor of two. Although arguments involving the extensional flow near the central planar extension point/line have been put forward to explain the destabilizing effect of the polymer additives, no quantitative theory has been developed by these authors. Using polyisobutylene/polybutene Boger fluids in an eccentric cylinder coater, Grillet, Lee & Shaqfeh (1999) demonstrated that the critical onset of ribbing in viscoelastic liquids can be directly correlated to a dimensionless elasticity parameter  $N = \lambda\sigma/\mu h$ , where  $h$  is a length scale of the flow geometry. The importance of the extensional behaviour of polymeric fluids to coating instabilities was studied by Soules, Fernando & Glass (1988), who concluded that an increase in extensional viscosity leads to reduced critical conditions for the onset of viscous fingering.

This paper continues an ongoing investigation of elastically driven free surface phenomena, with special emphasis on gravity effects on interfacial dynamics. To begin, we present experimental observations of how elasticity can affect the balance of forces in the menisci of interfacial flows. Digital particle image velocimetry (DPIV) and DEVSS finite element techniques are then used to investigate these flow fields.

## 2. Experimental apparatus

There have been numerous coating devices constructed to study the stability of interfacial flows. We present a design that is based on the eccentric-cylinder coater introduced by Rabaud *et al.* (1990) to study the Printer's instability. This setup consists of two horizontal cylinders of different radii with one placed inside the other (figure 2). The cylinders are mounted such that the eccentricity between them can be accurately controlled.

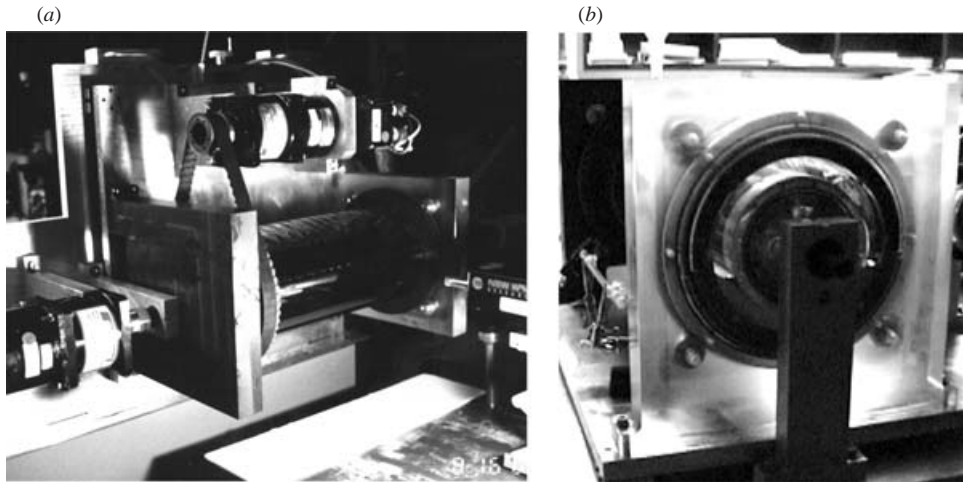


FIGURE 3. Eccentric-cylinder coating apparatus: Plexiglas outer cylinder (a) and acrylic end plate (b) for direct visualization of interfacial dynamics.

The outer cylinder, which has a radius of  $R_2 = 7.635$  cm, is machined and polished Plexiglas to allow complete visualization of the interface (figure 3a). One of the end plates supporting the cylinders is made out of acrylic material to permit an unhindered view of the cross-sectional interfacial profile and at the same time to allow application of the DPIV technique to investigate the flow field (figure 3b). Two aluminium inner cylinders of different radii (6 cm and 5.345 cm) are used to study the effect of confining walls on the formation of free surface singularities. The inner cylinders are black-anodized to facilitate flow investigation via DPIV and laser sheet imaging techniques. The surface roughness of the cylinders is measured to be less than  $10\ \mu\text{m}$  which should not affect the outcome of our experiments since the minimum gap width probed is  $\geq 500\ \mu\text{m} = 0.05$  cm. The cylinders are equal in length ( $L = 50$  cm) and their angular velocities ( $\omega_1, \omega_2$ ) are independently computer controlled. The axis of the inner cylinder can be shifted parallel to the axis of the outer cylinder such that eccentric cylinder flow can be generated. The minimum gap in our eccentric cylinder forward-roll coating experiments is denoted as  $b$  and ranged from 0.5 mm to  $b_{max} = 1.635$  cm (concentric cylinder forward-roll coating flow) when using the larger of the two inner cylinders ( $R_1 = 6$  cm). Although no special modification is made on the coating device to reduce the transverse flow off the ends of the cylinders, the dimensionless length of our experimental system,  $2L/(R_1 + R_2)$ , approaches 8 so we expect the influence of end effects on our experiments to be minor based on the conclusions drawn from previously published studies (Coyle *et al.* 1990; deBruyn & Pan 1995).

Although we have investigated extensively many types of coating flows, in this paper we will concentrate on the eccentric-cylinder forward-roll coating which we found to display the most interesting dynamics. In eccentric-cylinder forward-roll coating both cylinders are co-rotated at the same linear speed toward the air (figure 2) and hydrodynamic coatings are generated on the cylinder surfaces.

Two types of liquids were used in this study. The Newtonian liquid was an Amoco H-40 Indopol polybutene polymer with number averaged molecular weight near 750 and a viscosity of 110P, graciously donated by Amoco Chemical Company. In addition, a series of viscoelastic Boger fluids were made by mixing 0.1 to

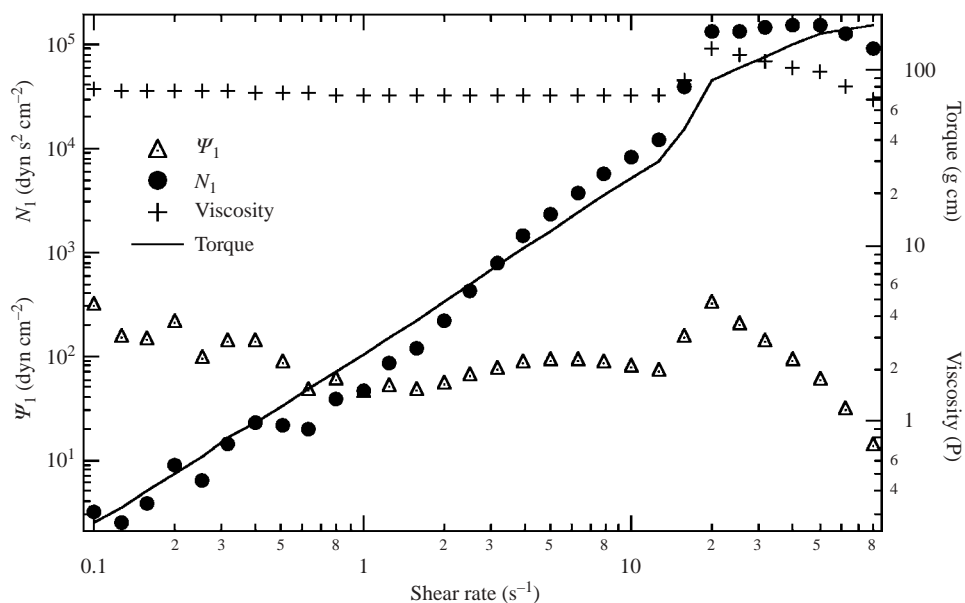


FIGURE 4. Rheological characterization of 0.1 wt% PIB/PB Boger fluid.

0.3 wt% high-molecular-weight polyisobutylene (Scientific Polymer Products, Inc., number average molecular weight,  $M_n = 4\,700\,000$ ) into a combination of  $\approx 3.5$  wt% kerosene (Aldrich) and  $\approx 96.4$  wt% polybutene (Amoco Chemical Co.). The viscosity of the final solution was varied in the series by using polybutene solvents with different viscosities. These different polybutene solvents were created by combining the H-40 Indopol product with H-100 Indopol polybutene ( $M_n = 940$ ,  $\mu \approx 215$  P) in different proportions. A measure of the high-molecular-weight polymer concentration in the solution is provided by the parameter  $S$ , which is defined as the ratio of the solvent viscosity to the total viscosity

$$S = \frac{\eta_s}{\eta_s + \eta_p}. \quad (2.1)$$

The series of Boger fluids employed in this study were then characterized by using a Rheometrics Dynamic Analyzer II, strain controlled rheometer. The pure polybutene exhibited a constant shear viscosity and no measurable normal force over a wide range of shear rates ( $0.1$ – $50$   $s^{-1}$ ). Figure 4 shows the rheological measurements of one of the PIB/PB Boger fluids, where we see that the first normal stress coefficient,  $\psi_1$ , plateaus over a decade of shear rates ( $2$ – $10$   $s^{-1}$ ) while the shear viscosity remains constant over three decades ( $0.1$ – $30$   $s^{-1}$ ), i.e. it exhibits the characteristics of ideal elastic fluids (Larson 1988; Boger & Mackay 1991). Similar behaviour was detected in the rheological characterization of a PS/DOP (polystyrene based) Boger fluid. The first normal stress coefficient plateau for the PS/DOP liquid spanned over two decades of shear rates ( $1$ – $20$   $s^{-1}$ ) and no shear thinning was observed for shear rates below  $20$   $s^{-1}$ . The relaxation times of the Boger fluids were determined in two ways: by fitting the decay of the normal stress after steady shear to a single exponential (figure 5) and by performing the Maxwell multimode fitting of the linear viscoelastic frequency sweep data (figure 6) via the Levenberg–Marquardt nonlinear regression method (Edgar & Himmelblau 1988). The inadequacy of using a single-mode model to describe the linear viscoelastic response of the fluid is evident in

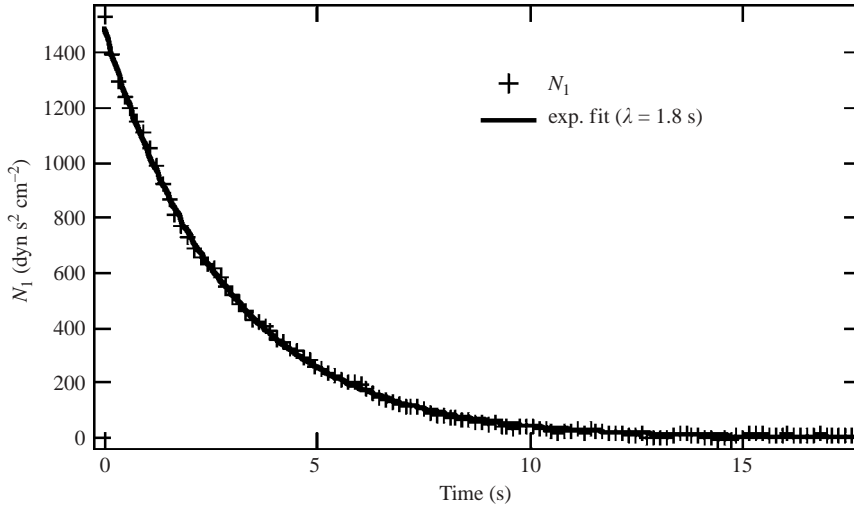


FIGURE 5. Relaxation time estimation by fitting normal stress decay after steady shear to a single exponential (0.1 wt% PIB/PB Boger fluid).

figure 6. Rheological experiments using highly monodisperse polymeric systems have shown that a single relaxation time is insufficient to describe the many different modes of relaxation available to long flexible polymer chains (Larson 1988). This problem can be solved by introducing multiple time constants (Bird, Armstrong & Hassger 1987) to characterize the relaxation modulus as

$$G(t) = \sum_{k=1}^{\infty} \frac{\eta_k}{\lambda_k} e^{-t/\lambda_k}. \quad (2.2)$$

For each of the elastic fluids used in our study, their linear viscoelastic responses can be accurately captured by using four relaxation time constants (figure 6). Moreover, fairly good agreement is found between the relaxation times obtained by normal stress decay fitting procedure and the longest relaxation modes computed via the multimode fitting for all liquids used in this study, as shown in table 1. While both procedures only give an approximation to the longest relaxation time in a spectrum of relaxation times possessed by any real viscoelastic liquid, the relaxation time determined from the decay of normal stress has been found elsewhere in the literature to correlate the occurrence of purely elastic instabilities (Magda & Larson 1988; Larson *et al.* 1990).

The rheological characterization tests were performed for the range of temperatures used in our experiments (19°C–21°C), so the temperature dependence of the viscosity and relaxation times have been taken into account when calculating the Weissenberg and capillary numbers for each experiment. Surface tension was measured by using a Wilhelmy balance and was found to be constant within the experimental errors for the range of temperatures in which our experiments were conducted. To get a measure of the elasticity of each of the Boger fluids which is not dependent on the cylinder rotation velocity or experimental gap width,  $b$ , we define an elasticity parameter  $N$  as the ratio of the Weissenberg number and the capillary number.

$$N = \frac{U\lambda/b_{nom}}{\mu U/\sigma} = \frac{\lambda\sigma}{\mu b_{nom}}. \quad (2.3)$$

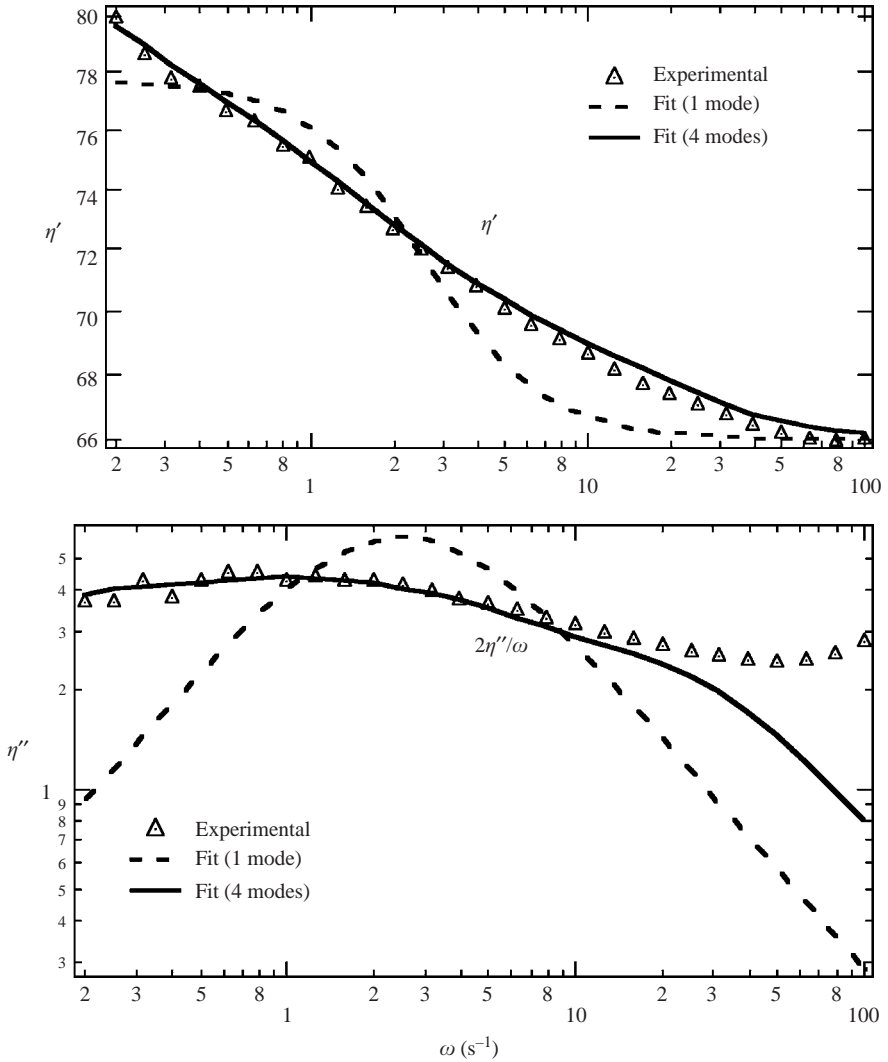


FIGURE 6. Relaxation time estimation via Maxwell multimode fitting of dynamic viscosity,  $\eta'$ , and dynamic rigidity,  $\eta''$  (0.1 wt% PIB/PB Boger fluid).

Note that  $N$  is defined using the nominal gap width of  $b_{nom} = 10$  mm in order to keep the parameter constant for a series of experiments at varying gap widths. The relaxation times estimated from the normal stress relaxation experiments were used to determine the elasticity parameter value for each liquid. The parameter  $N$  was first suggested by Ro & Homsy (1996) to study the flow of a viscoelastic liquid in a divergent channel. Physically this parameter can be thought of as the ratio of the polymer relaxation time and the time for an interface deformed by an amount  $b_{nom}$  to relax under surface tension. The fluids used in our experiments spanned  $N$  values from 0 (Newtonian liquid) to 2.12 (semi-dilute polymer concentration regime). Table 1 presents the physical properties of the liquids used in this work listed in order of increasing  $N$  values. As can be seen from the surface tension values listed in table 1, there is no systematic change in the mechanical properties of the fluid interfaces due to the addition of polymers.



Fluid	$\rho$ (g cm <sup>-3</sup> )	$\sigma$ (dyn cm <sup>-1</sup> )	$\eta$ (P)	$\Psi_1$ (dyn cm <sup>-1</sup> / dyn s <sup>2</sup> cm <sup>-2</sup> )	$S$	$\lambda_{stress\ relax.}$ (s)	$\lambda_{Relax. Spect.}$ 4 modes (s)	
PB ( $N=0$ )	0.88	29.4 ± 2	103.8 ± 5	0.0	1.0	0.0	0.0	
PIB/PB ( $N=0.39$ )	0.88	30.0 ± 2	161.1 ± 5	50.0	0.88	2.1	3.47 0.4	2.94 0.04
PIB/PB ( $N=0.53$ )	0.88	33.0 ± 2	210.2 ± 5	155.0	0.85	3.3	4.5 0.14	0.82 0.03
PIB/PB ( $N=0.78$ )	0.88	32.8 ± 2	237.9 ± 5	235.0	0.89	5.7	8.5 0.24	1.42 0.03
PIB/PB ( $N=0.87$ )	0.88	32.0 ± 2	117.0 ± 5	80.0	0.85	3.2	4.17 0.2	0.98 0.04
PS/DOP ( $N=1.07$ )	0.88	29.0 ± 2	95.0 ± 5	55.0	0.75	3.5	4.95 0.16	0.73 0.03
PIB/PB ( $N=1.08$ )	0.88	30.0 ± 2	50.0 ± 5	50.0	0.87	1.8	3.5 0.25	0.92 0.04
PIB/PB ( $N=2.08$ )	0.88	30.0 ± 2	180.0 ± 5	1050.0	0.52	12.5	13.89 0.37	2.30 0.04
PIB/PB ( $N=2.12$ )	0.88	30.0 ± 2	130.1 ± 5	400.0	0.73	9.2	10.5 0.37	2.03 0.04

TABLE 1. Rheological properties of the fluids at room temperature (21 °C).

### 3. Experimental results

We shall begin our discussion of the effects of elasticity on the dynamics of interfaces in air  $\Rightarrow$  liquid displacement flows by presenting our experimental results on the eccentric forward-roll coating flow. This flow has been the most widely studied by previous researchers (Coyle *et al.* 1990), and is one of the few such flows which has been investigated with viscoelastic liquids (Bauman *et al.* 1982; Soules *et al.* 1988; Fernando & Glass 1988, Dontula *et al.* 1996; Grillet *et al.* 1999). In addition, the theoretical dispersion relationship and critical conditions derived for Newtonian Hele-Shaw flows (Saffman & Taylor 1958) can be modified to analyse, as a first approximation, the stability of forward-roll coating due to the similarity in their flow fields. The results of our studies with other coating flow geometries can be found in Lee (2001).

#### 3.1. Eccentric-cylinder forward-roll coating

One of the most intensely researched viscoelastic interfacial phenomena, due to its importance in industrial coating applications, is the variation of coating film thickness (Bonn *et al.* 1995; Huzyak & Koelling 1997; Lee *et al.* 2002) as a function of the processing speed.

Our film thickness measurements are shown in figures 7(a) and 7(b), where the dimensionless film thickness or fractional coverage,  $m$ , is plotted as a function of  $Ca$  for the Newtonian fluid in figure 7(a) and as a function of  $Gr$  in figure 7(b) for both Newtonian and elastic Boger fluids. The dimensionless film thickness/fractional coverage,  $m$ , is defined as

$$m = \frac{b_{channel} - b_{air}}{b_{channel}} \quad (3.1)$$

where  $b_{channel}$  is the width of the channel measured at the meniscus and  $b_{air}$  is the width of the two-dimensional air bubble measured far downstream from the

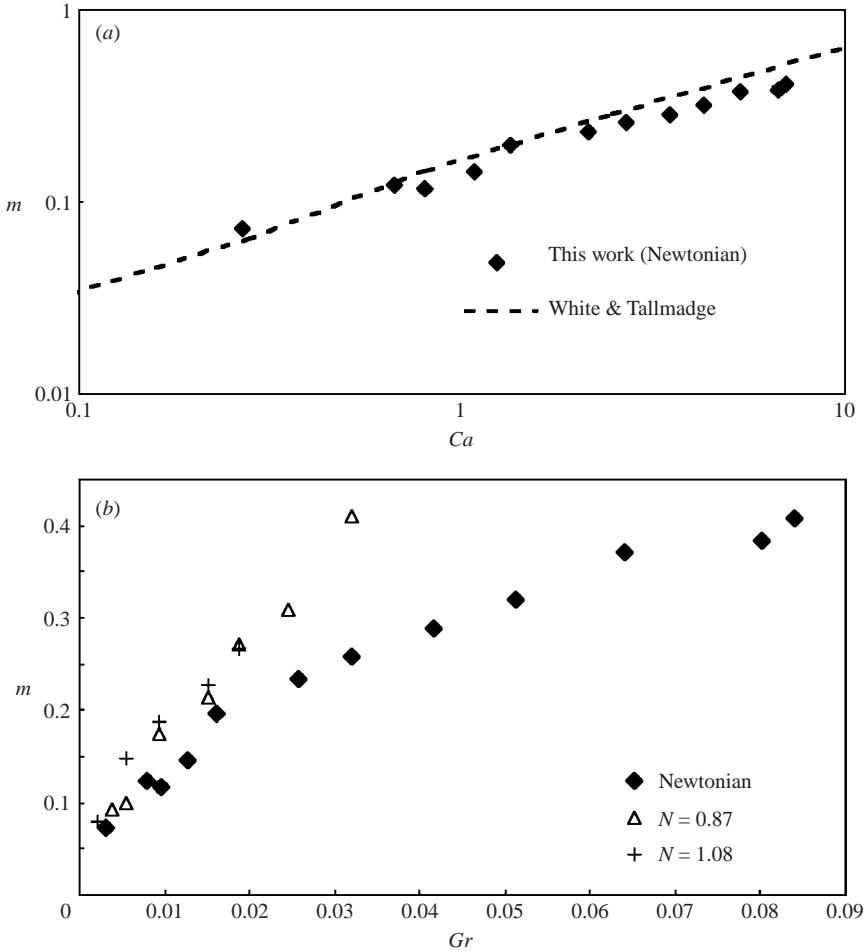


FIGURE 7. Measured dimensionless coating film thickness/fractional coverage: (a) fractional coverage as a function of capillary number: Newtonian liquid; (b) fractional coverage as a function of gravity number: Newtonian vs. elastic Boger fluids ( $N = 0.87$  and  $N = 1.08$ ).

meniscus. Included in figure 7(a) for comparison is the film thickness prediction from the theory of drag out of liquids on flat plates or dip coating in the gravity-dominated flow regime (White & Tallmadge 1965; Tharmalingam & Wilkinson 1978). Looking first at the Newtonian liquid data, figure 7(a) shows good agreement between our measurements and the gravity-corrected theoretical predictions derived for dip coating, thus confirming that our experiments were in fact conducted in the gravity-dominated regime. Our film measurements (figure 7b) show that deviation from Newtonian behaviour begins at lower values of  $Gr$  as the elasticity of the liquid increases. For  $0 \leq Gr \leq 0.005$ , the flow Weissenberg numbers were found to be below 0.5. Note that the Bond number,  $Bo$ , is held fixed in these measurements (concentric-cylinder forward-roll coating flow) so the changes in  $Gr$  are directly correlated with the changes in flow  $Ca$ , i.e. the cylinder rotation speed. The measurements were not continued at higher values of  $Gr$  than those shown due to the onset of ribbing instabilities. It is important to point out that significant film thickening was observed in our experiments for values of  $Wi$  as low as 0.25 whereas flow experiments

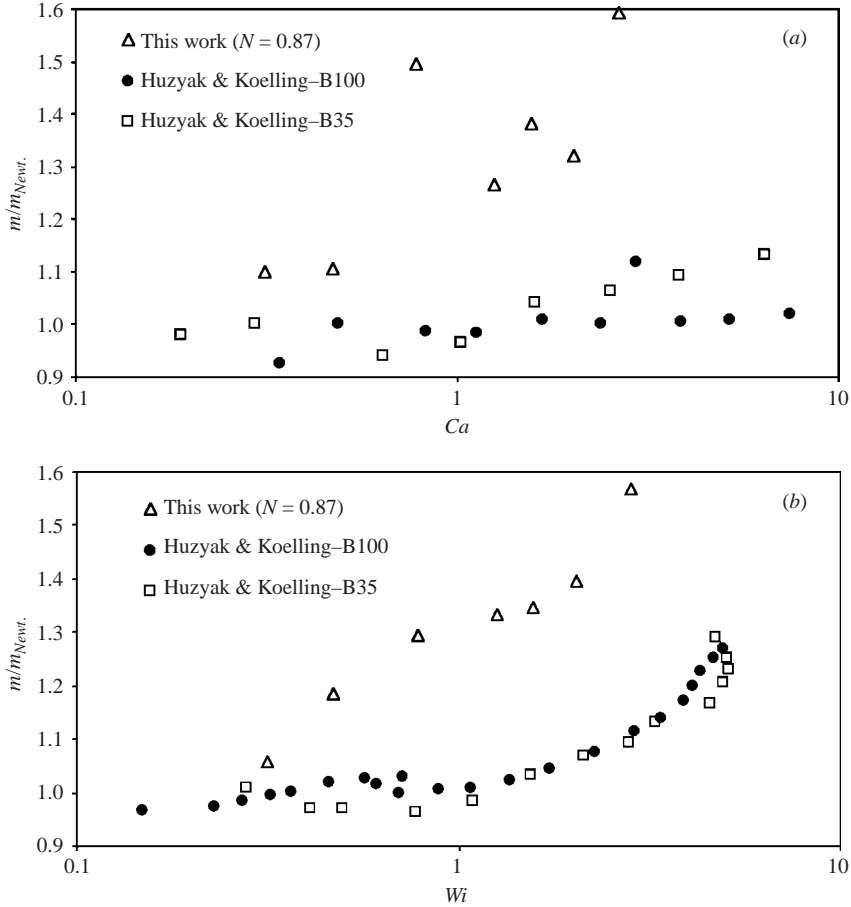


FIGURE 8. Comparison of the reduced fractional coverage,  $m/m_{Newt.}$ , as a function of (a)  $Ca$  and (b)  $Wi$  between data obtained in this study and those measured by Huzyak & Koelling (1997) in a horizontally positioned ( $Bo = 0$ ) capillary tube.

conducted in a horizontal capillary tube ( $Bo = 0$ ) by Huzyak & Koelling (1997), also with PIB/PB elastic Boger fluids, have reported little elasticity-driven film variation for values of  $Wi$  below 1.0 as shown in figure 8(b). The same set of data plotted as a function of flow  $Ca$  is shown in figure 8(a).

A laser sheet study of the air–liquid interface (using the larger of the two inner cylinders, i.e.  $R_1 = 6$  cm) for elastic fluids at increasing values of the capillary number before the onset of ribbing instability revealed the formation of a stable two-dimensional ‘sharp interface’ along the centre stagnation line of the meniscus when the dimensionless gap separation between the cylinders ( $b/b_{max}$ ) is greater than 0.7, where  $b_{max}$  is again the difference between the inner and outer cylinder radii ( $R_2 - R_1 = 1.635$  cm), as defined in the previous section. The experimental flow parameters for the elastic Boger fluid interfacial evolution shown in figure 9(d–f) are: (d)  $Ca = 0.25$ ,  $Gr = 0.003$ ,  $Wi = 0.2$ ; (e)  $Ca = 0.913$ ,  $Gr = 0.011$ ,  $Wi = 0.6$ ; (f)  $Ca = 1.73$ ,  $Gr = 0.021$ ,  $Wi = 1.0$ . The Bond number is again held constant ( $Bo = 83$ ) in this set of experiments (concentric-cylinder forward-roll coating flow). The interfacial evolution for a Newtonian liquid under similar flow conditions is shown in figure 9(a–c). While highly deformed menisci are also detected in the Newtonian case at higher values of  $Gr$  (figure 9c), for

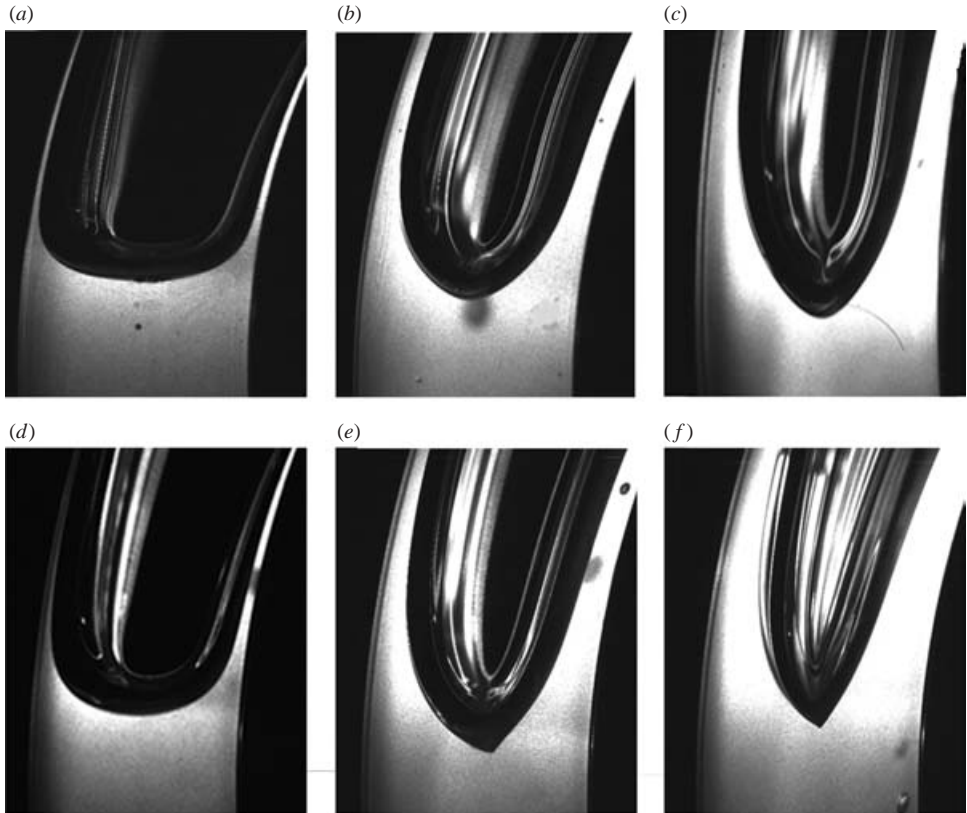


FIGURE 9. Experimentally observed interfacial evolution for both Newtonian (*a-c*) and viscoelastic liquids (*d-f*) ( $b_{max} = 1.635$  cm,  $Bo = 83$ ): (*a*)  $Ca = 0.25$ ,  $Gr = 0.003$ ; (*b*)  $Ca = 0.913$ ,  $Gr = 0.011$ ; (*c*)  $Ca = 1.73$ ,  $Gr = 0.021$ ; (*d*)  $Ca = 0.25$ ,  $Gr = 0.003$ ,  $Wi = 0.2$ ; (*e*)  $Ca = 0.913$ ,  $Gr = 0.011$ ,  $Wi = 0.6$ ; (*f*)  $Ca = 1.73$ ,  $Gr = 0.021$ ,  $Wi = 1.0$ .

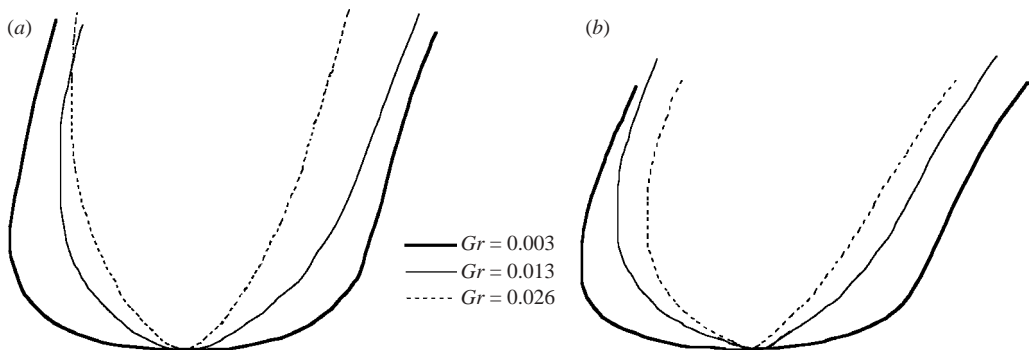


FIGURE 10. Analysis of the interfacial profile evolution for (*a*) Newtonian and (*b*) viscoelastic liquids.

the flows considered in this study the surface tension force apparently is always dominant and the formation of free surface singularities is restrained. A more quantitative measure of the interfacial deformation as a function of  $Gr$  is shown in figure 10, where the digital images captured in our experiments are analysed via edge detection software.

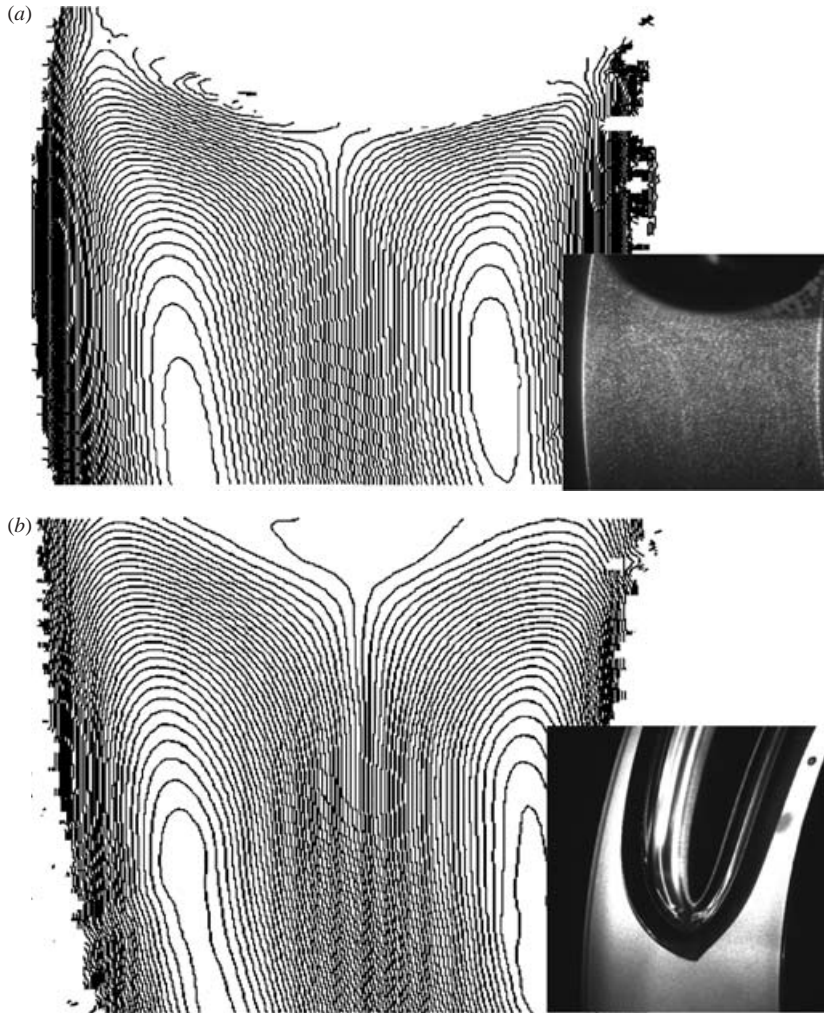


FIGURE 11. Flow streamlines for (a) Newtonian and (b) viscoelastic liquids obtained using DPIV for  $Gr=0.013$  ( $Ca=0.913$ ).

The mechanism of formation of this newly discovered, two-dimensional ‘sharp interface’ in viscoelastic liquids under creeping flow conditions is not immediately clear. In the case of cusp formation observed at the trailing edge of a bubble rising in a viscoelastic liquid the most cited mechanism is based on the phenomenon of ‘negative wake’ formation behind the bubble (Hassager 1979), which suggests that extensional forces due to polymer additives tend to pull out a cusp against the restraining action of surface tension (Jeong & Moffatt 1992; Joseph & Feng 1995; Liu, Liao & Joseph 1995). Furthermore, Joseph *et al.* (1991) and Jeong & Moffatt (1992) showed that the shape of the free surface near the cusp is universally  $y=ax^{2/3}$  and that the resulting radius of curvature at the cusp tip due to surface tension rounding is exponentially small, of the order of hundreds of angstroms at capillary number of order unity. To check whether a similar mechanism applies in our situation, the digital particle image velocimetry (DPIV) technique is used to visualize the flow field. Figure 11 shows the streamlines obtained from our DPIV

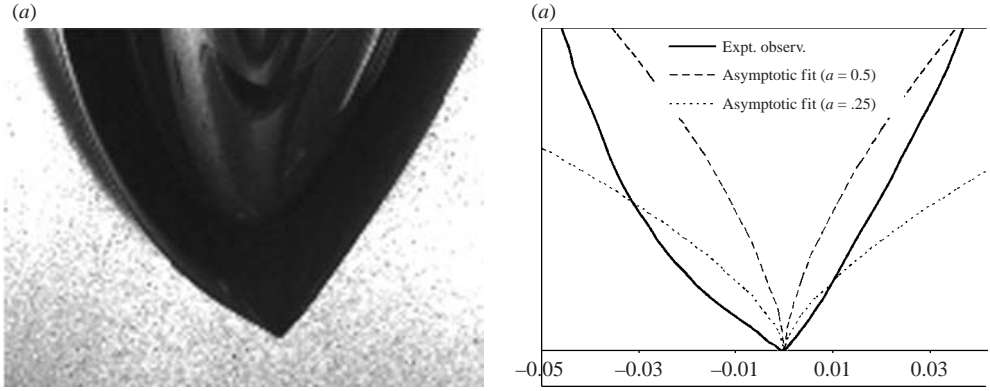


FIGURE 12. (a) Close-up of the two-dimensional sharp interface for  $Ca = 0.913$ ,  $Gr = 0.013$ ,  $Wi = 0.6$  ( $b_{max} = 1.635$  cm,  $Bo = 83$ ). (b) Comparison between the shape of the experimentally observed sharp interface and the asymptotic relation  $y = ax^{2/3}$  for cusps.

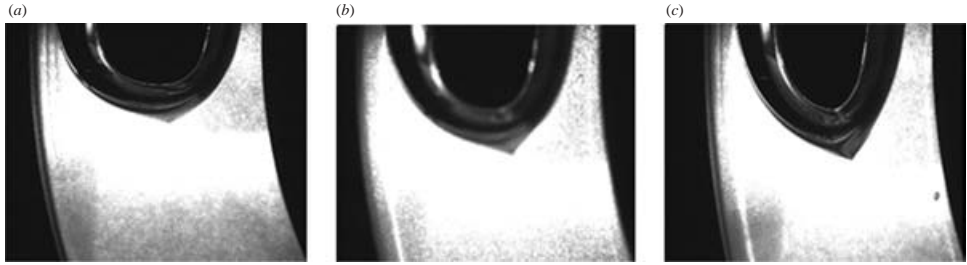


FIGURE 13. Meniscus dynamics for elastic liquid (gap width = 2.3 cm,  $Bo = 117$ ): (a)  $Ca = 1.33$ ,  $Gr = 0.009$ ,  $Wi = 0.74$ ; (b)  $Ca = 1.6$ ,  $Gr = 0.01$ ,  $Wi = 0.89$ ; (c)  $Ca = 2.13$ ,  $Gr = 0.014$ ,  $Wi = 1.18$ .

experiments for both Newtonian (figure 11a) and elastic liquids (figure 11b) for  $Gr = 0.013$  ( $Ca = 0.913$ ). In the streamlines for the viscoelastic liquid (figure 11b), the strong deformation of the interface along the centre planar extension line can be readily observed which suggests that the cusping mechanism based on ‘negative wake’ formation may also be applicable to the two-dimensional ‘sharp interface’ encountered in our experiments. However, when the laser sheet image is magnified near the tip of the two-dimensional ‘sharp interface’ (figure 12a, b) we detect a near zero or positive-curvature interface rather than the traditional negative-curvature cusp structure dictated by the universal asymptotic relation  $y = ax^{2/3}$  (figure 12b). One important distinction between our experiments and those involving a bubble rising in a viscoelastic liquid is the closeness of the two-dimensional air bubble to the confining walls/cylinders in our experimental geometry. To see if the proximity of the walls had a significant effect on the shape of the sharp interface witnessed in our experiments, the concentric forward-roll coating experiment with a viscoelastic liquid is repeated using the smaller of the two inner cylinders ( $R_1 = 5.345$  cm) which increases  $b_{max}$ , i.e. the gap width, by 40%. The interfacial evolution observed from this new set of experiments is shown in figure 13(a–c): (a)  $Ca = 1.33$ ,  $Gr = 0.0086$ ,  $Wi = 0.74$ ; (b)  $Ca = 1.6$ ,  $Gr = 0.01$ ,  $Wi = 0.89$ ; (c)  $Ca = 2.13$ ,  $Gr = 0.014$ ,  $Wi = 1.18$ . A two-dimensional sharp interface is again formed at the meniscus and a magnified view of the sharp interface tip is shown in figure 14(a). Figure 14(b) shows that the interface shape at higher  $b_{max}$  value is apparently consistent with the  $y = ax^{2/3}$



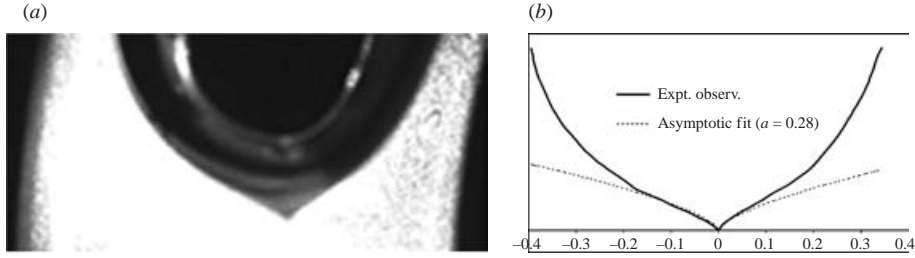


FIGURE 14. (a) Close-up of the two-dimensional sharp interface for  $Ca = 1.6$ ,  $Gr = 0.01$ ,  $Wi = 0.89$ ; ( $b_{max} = 2.3$  cm,  $Bo = 117$ ). (b) Comparison between the experimentally observed cusp and the asymptotic relation  $y = ax^{2/3}$  describing cusps.

shape described by Joseph *et al.* (1991) for cusps. Further investigation is needed to determine how the elastic stress fields vary with gap width in order to understand the formation of the differing sharp interface shapes witnessed in our experiments at high values of  $Wi$  and  $Ca$ . We note, in other related research, that a steady two-dimensional cusp was discovered by Joseph *et al.* (1991) by rotating a cylinder half immersed in a viscous Newtonian liquid. They detected the formation of a two-dimensional cusp at the contact line (stagnation line if the interface is rounded) between the impinging fluid film and the fluid reservoir at finite cylinder rotation speeds.

It has been observed in our experiments that as the rotation speed of the cylinders is increased slightly above that at which the two-dimensional sharp interface is first observed, the tip of the sharp interface, i.e. the centre stagnation line marked by the circle in figure 15(a), breaks up into evenly spaced, millimetre sized, substructures. Magnifications of the top- (figure 15b, c) and side-views (figure 15d) along the tip of the two-dimensional sharp interface shows that the newly formed interfacial substructures are three-dimensional in nature and resemble an array of inverted, elongated cones (figure 15d). The most unusual aspect of these substructures is their stability with respect to further increases in  $Ca$ . Neither the amplitude nor the wavelength undergoes changes with increasing rotation speed of the cylinders. In fact, these substructures persist in their initial form even during the critical onset of viscous fingering. It is worth pointing out that the formation of stable interfacial substructures has been observed before in surfactant driven instability (SDI) experiments (Guo, Hong & Kurtze 1992; Chan & Liang 1997; Chan 2000).

Next we report on the investigation of the interfacial stability for a range of dimensionless minimum gap widths,  $b/R$ , where  $R$  is the average of the inner and outer cylinder radii and is the length scale used to determine the flow capillary number. For  $Ca$  at which the flow is stable, viscous forces would produce a smooth hydrodynamic coating film on the surface of the cylinders. Above the critical  $Ca$ ,  $Ca_{crit}$ , undulations appear on the interface which thereafter grow in amplitude to form fingers. These critical conditions are plotted versus the dimensionless gap ratio in figures 16(a) and 16(b). Our one-dimensional stability analysis with film flow stabilization accurately captured the critical conditions for the onset of Newtonian viscous fingering (Grillet *et al.* 1999). For the weakly elastic liquid,  $N = 0.39$ , there is no measurable change in the critical conditions over the Newtonian liquid flow. However, for the more elastic liquids,  $N > 0.7$ , there is a very significant decrease in the critical speed for the onset of instability causing the critical capillary number,  $Ca_{crit}$ , to fall by a factor of three for the largest gap widths, i.e. when approaching concentric cylinder forward-roll coating flow. The results can also be presented in terms of the gravity number,  $Gr$ , where the

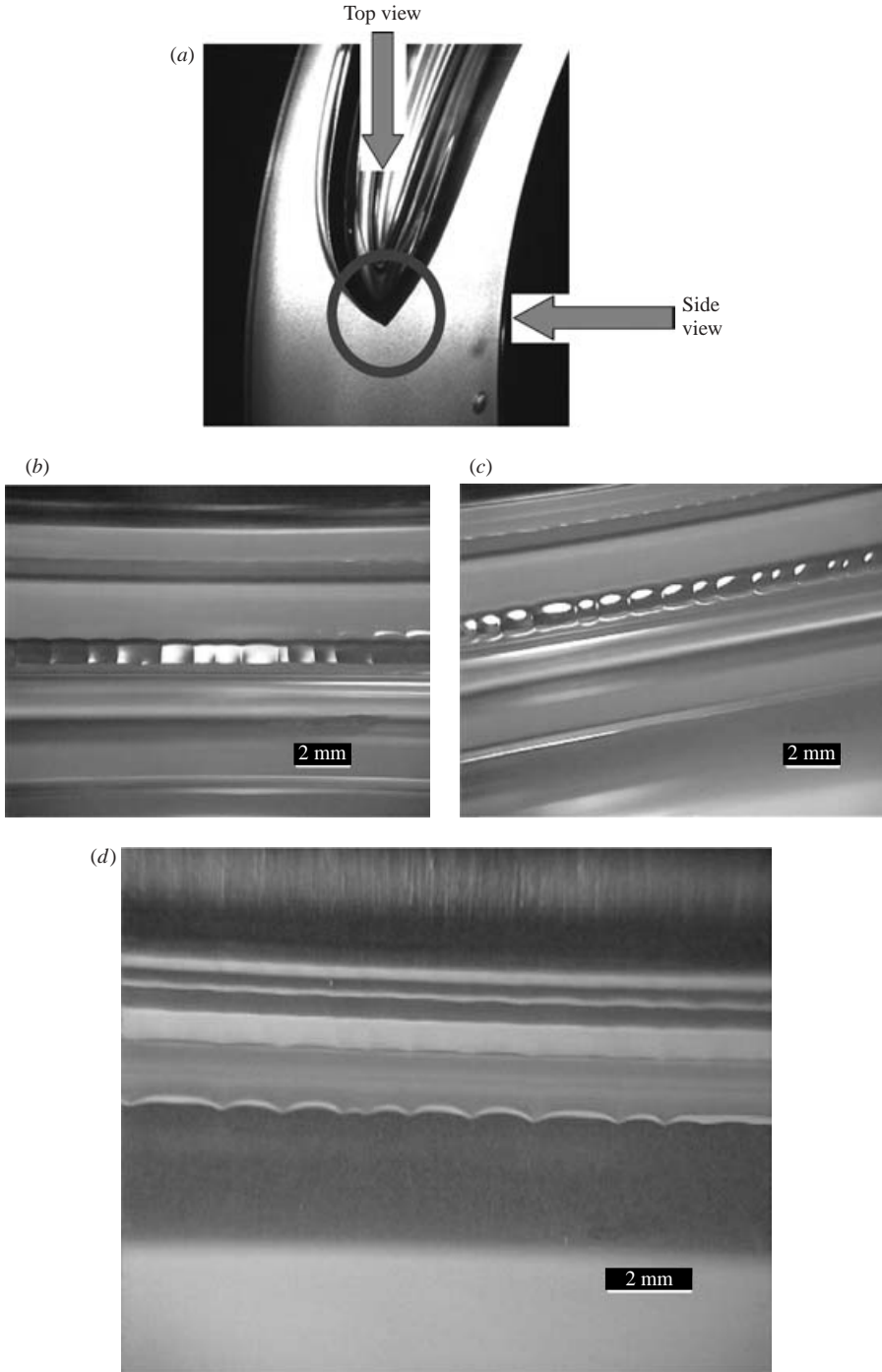


FIGURE 15. Substructure formation at the tip of the sharp interface: (a) location of the millimetre sized substructures; (b, c) top-view magnification of the substructures; (d) side-view magnification showing the elongated conical shape of the substructures.



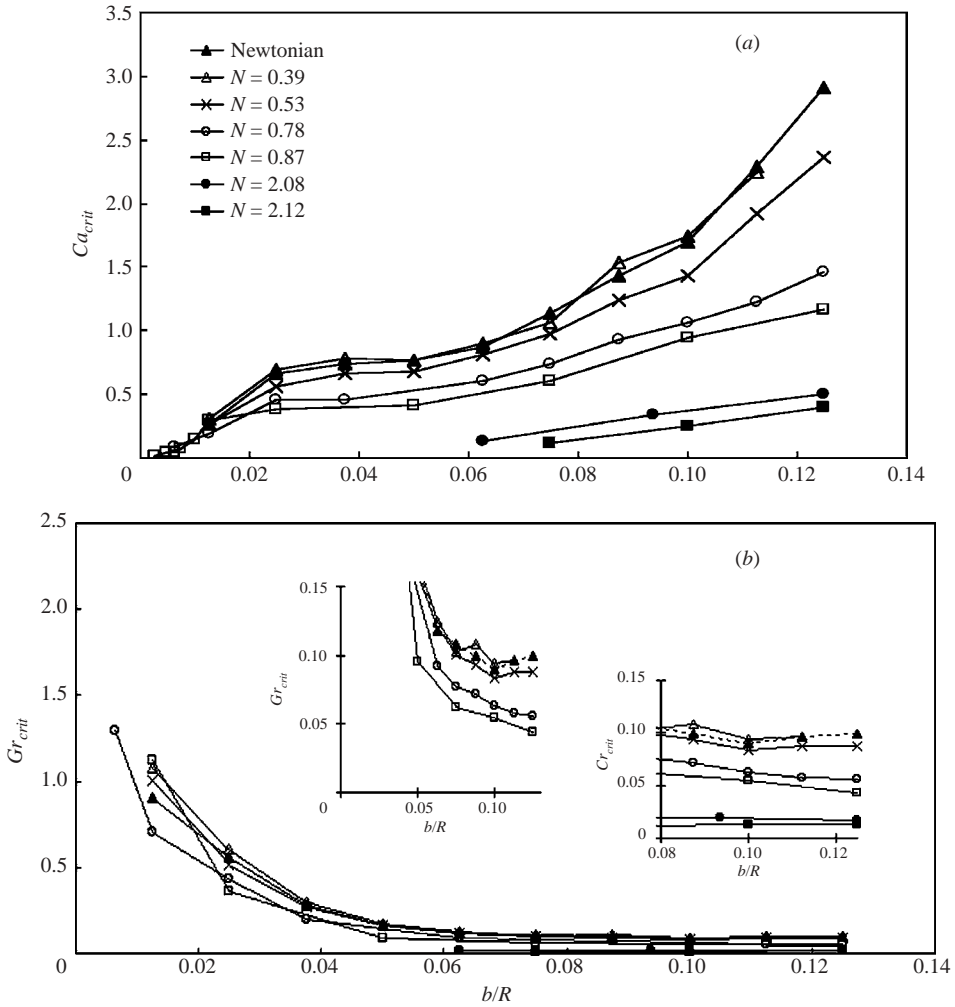


FIGURE 16. Stability curves for both Newtonian and viscoelastic liquids: (a) critical capillary number,  $Ca_{crit}$ , vs. dimensionless gap width,  $b/R$ ; (b) critical gravity number,  $Gr_{crit}$ , vs. dimensionless gap width,  $b/R$ .

destabilization for the elastic liquids with  $N > 0.7$  occurs as a near constant shift of the critical values by a factor of 2–4 over the entire range of gap ratios (figure 16b). This destabilization due to gravity effects is explored in our numerical simulations and the results will be presented in the next section. No comparison is presented between our results and those from previous researchers because our experiments were mostly conducted in the gravity-dominated regime while previous works had exclusively focused on the surface-tension dominated regime. Our experiments at smaller gap widths (the lower portion of our data) approach the other data as the surface tension stabilization becomes comparable to the gravity stabilization in our experiments (Grillet *et al.* 1999). The monotonic decrease in critical conditions with increasing elasticity parameter is tested by increasing the concentration of the high molecular weight polymer in the solution to almost  $3c^*$  (0.3 wt%), i.e. three times the critical concentration of entanglement ( $N = 2.12$ ). As shown in figure 16(a, b), the

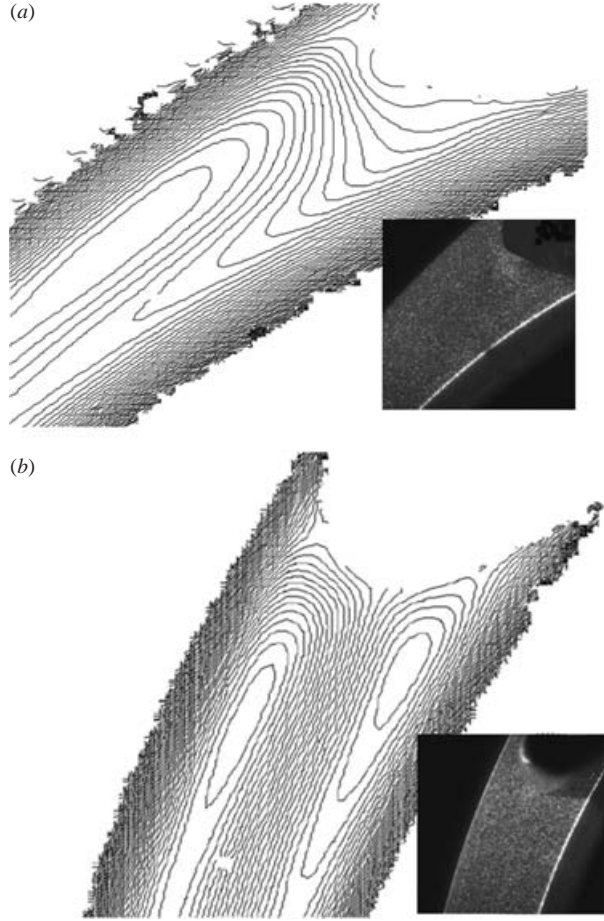


FIGURE 17. Flow streamlines obtained using DPIV for (a)  $b/b_{max} = 0.06$ ,  $Gr = 0.79$  and (b)  $b/b_{max} = 0.6$ ,  $Gr = 0.02$ .

observed trend still holds for fluids with polymer concentration in the semi-dilute regime. It is worth mentioning that a monotonic increase in critical wavenumber with increasing fluid elasticity has also been observed in our experiments. This phenomenon has been explored in detail in our previous paper (Grillet *et al.* 1999).

As stated in the introduction, the increase in extensional viscosity due to the presence of a stagnation point/line on the free surface has often been identified as the main driving force for the onset of fingering instabilities in viscoelastic liquids (Bauman *et al.* 1982). The DPIV technique is used to visualize the flow fields at various gap separations and to determine the location of the stagnation line(s) on the free surface. A sample of the results is shown in figure 17. While for larger gap separations ( $b/b_{max} \geq 0.4$ ) the flow field is mostly symmetric with respect to the centre stagnation line (figure 17b), this symmetry is broken in highly eccentric flows (figure 17a). The number of stagnation lines on the free surface is reduced from 3 in nearly concentric flows to 1 in highly eccentric flows and its location is displaced far away from the meniscus region. Further investigation is needed to determine how this change in the flow field affects the stress distribution near the free surface and the stability of the interface.

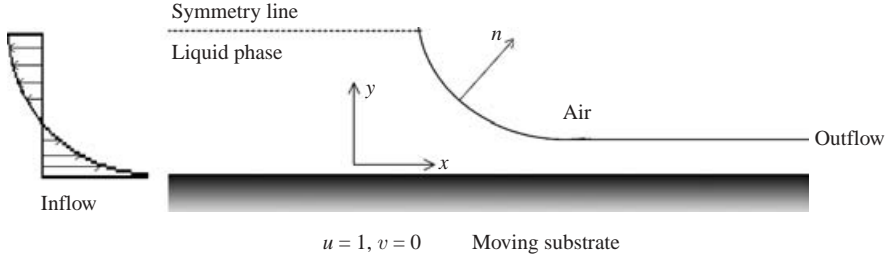


FIGURE 18. Gas-assisted liquid displacement in planar flow geometry.

#### 4. Mathematical formulation

Although the problem of viscoelastic free surface flows has been studied in detail in our previous paper (Lee *et al.* 2002), the richness of interfacial phenomena observed in our experiments prompts us to repeat the numerical analysis to examine the effect of gravity on interfacial evolution. The mathematical formulation is briefly reintroduced below for completeness.

##### 4.1. Governing equations

The two-dimensional steady elastic free surface problem depicted in figure 18 is defined by the governing equations which impose conservation of mass and momentum for an incompressible fluid in these geometries:

$$\nabla \cdot \mathbf{u} = 0, \quad (4.1)$$

$$Re \mathbf{u} \cdot \nabla \mathbf{u} = -\frac{\nabla P}{Ca} + \nabla \cdot \boldsymbol{\tau}, \quad (4.2)$$

where  $Re$  is the Reynolds number and is defined as

$$Re = \frac{\rho U b}{\eta} \quad (4.3)$$

where  $\rho$  is the density of the fluid,  $\eta$  is the total viscosity of the fluid and  $U$  is the characteristic velocity of the problem. In this paper, only the creeping flow regime,  $Re = 0$ , is analysed, and  $\mathbf{u}$  is the velocity vector,  $P$  is the pressure and  $\boldsymbol{\tau}$  is the total stress tensor formed by the sum of the Newtonian solvent stress,  $\boldsymbol{\tau}^s$ , and the polymer stress,  $\boldsymbol{\tau}^p$ . The basic equations are non-dimensionalized as

$$(x, y) [=] (b, b), \quad (u, v) [=] U, \quad P [=] T/b, \quad \boldsymbol{\tau} [=] \eta U/b,$$

where  $\eta$  is the total viscosity of the fluid at zero shear rate.

To analyse the physics of polymer stretching in these flows as well as to determine the flow field modification by the presence of polymers, the FENE-CR (Chilcott & Rallison 1988) model is chosen for our simulations because it adequately captures the rheological properties measured in Boger fluids (non-shear thinning, bounded extensional viscosity).

The constitutive models chosen can be separated into two parts: an evolution equation for the elastic dumbbells (upon which all these models are based), and an expression for the polymer stress. For the FENE-CR model, the dumbbells are taken to evolve in steady flow according to

$$\mathbf{u} \cdot \nabla \mathbf{A} = \mathbf{A} \cdot \nabla \mathbf{u} + \nabla \mathbf{u}^T \cdot \mathbf{A} - \frac{f(R)}{Wi} (\mathbf{A} - \mathbf{I}) \quad (4.4)$$

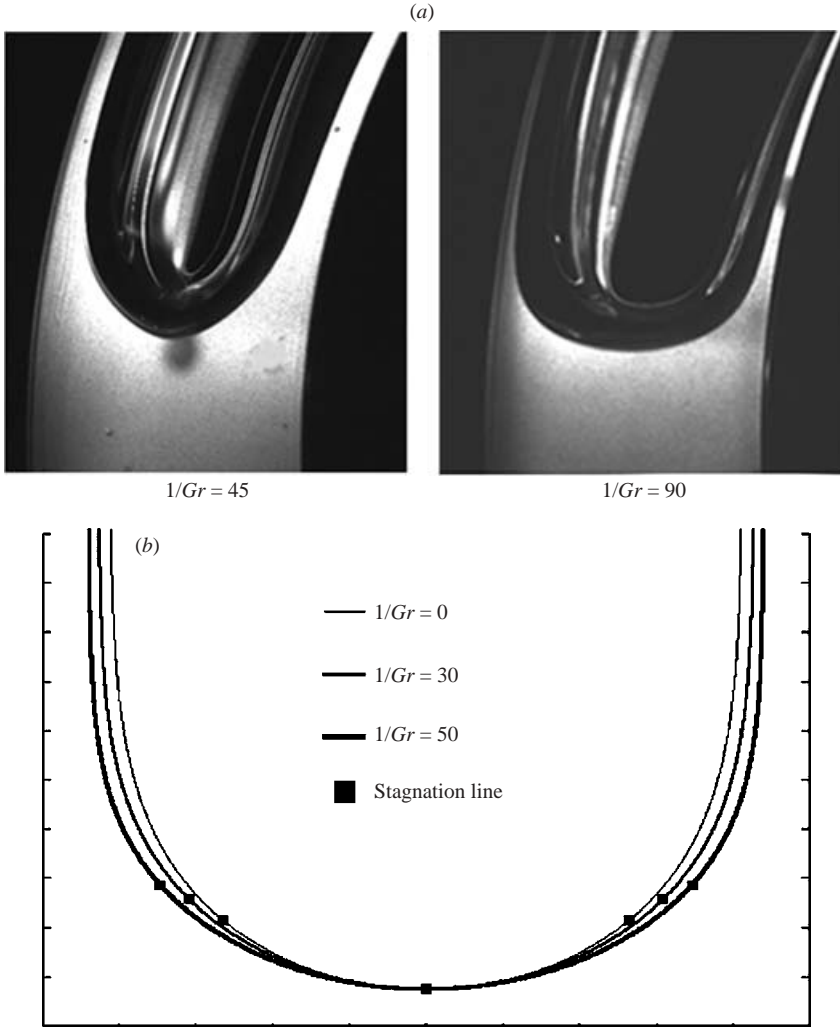


FIGURE 19. Gravity effects on the shape of the free surface: (a) experimental observations; (b) numerical predictions. The squares mark the locations of the stagnation lines.

in which  $\mathbf{A}$  represents an ensemble average of the dyadic product  $\mathbf{R}\mathbf{R}$  of the dumbbell end-to-end vector  $\mathbf{R}$ , and  $f(R)$  is the spring force law of the individual dumbbells. The spring force law,  $f(R)$ , is taken to be

$$f(R) = \frac{1}{1 - R^2/L^2} \quad (4.5)$$

where  $R^2$  is the trace of the polymer conformation tensor  $\mathbf{A}$  and  $L$  represents the ratio of the length of a fully extended polymer dumbbell to its equilibrium length. The polymeric contribution to the total stress for the FENE-CR model can be written as

$$\boldsymbol{\tau} = \underbrace{2S\dot{\boldsymbol{\gamma}}}_{\boldsymbol{\tau}^s} + \underbrace{\frac{(1-S)}{Wi} f(R)(\mathbf{A} - \mathbf{I})}_{\boldsymbol{\tau}^p} \quad (4.6)$$

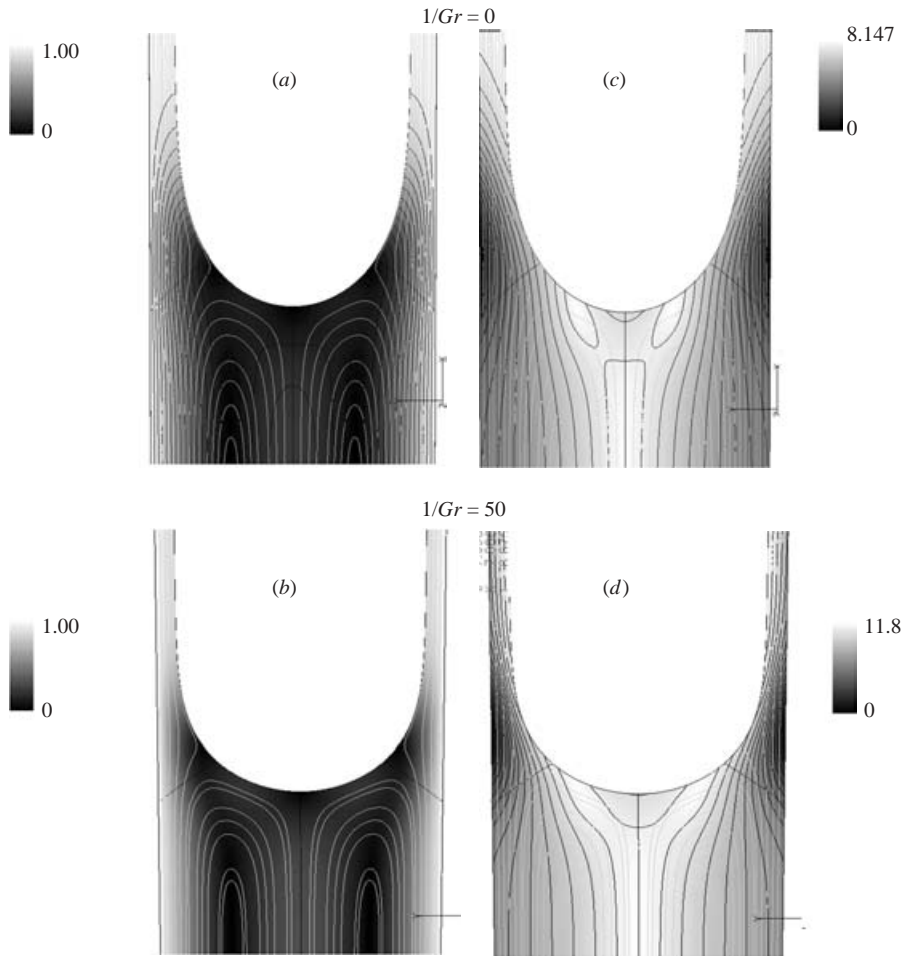


FIGURE 20. Numerical modelling of the gravity effects on the flow field (*a, b*) and the second invariant of the rate of strain tensor (*c, d*) for a Newtonian liquid ( $1/Gr = 0-50$  and  $Ca = 0.1$ ).

where the parameter  $S$  is the ratio of the solvent viscosity to the total viscosity and it provides a measure of the polymer concentration in the fluid.

These equations along with the appropriate free surface boundary conditions are solved via the DEVSS formulation proposed by Guenette & Fortin (1995). The details of the numerical solution can be found in Lee *et al.* (2002).

## 5. Computational results

Figure 19 shows a comparison between our experimental observations and numerical prediction of Newtonian interfacial evolution as a function of  $Gr$ . While the flattening of the meniscus shape with increasing gravity effects is hardly surprising, the significant displacement of the lateral stagnation lines toward the confining walls and the subsequent reduction in hydrodynamic coating film thickness (figure 19*b*) confirm a rapid strengthening of the recirculation flow due to gravity forces. The flow streamlines shown in figures 20(*a*) and 20(*b*), where the greyscale describes the magnitude of the local fluid flow velocity (normalized with respect to the wall speed),

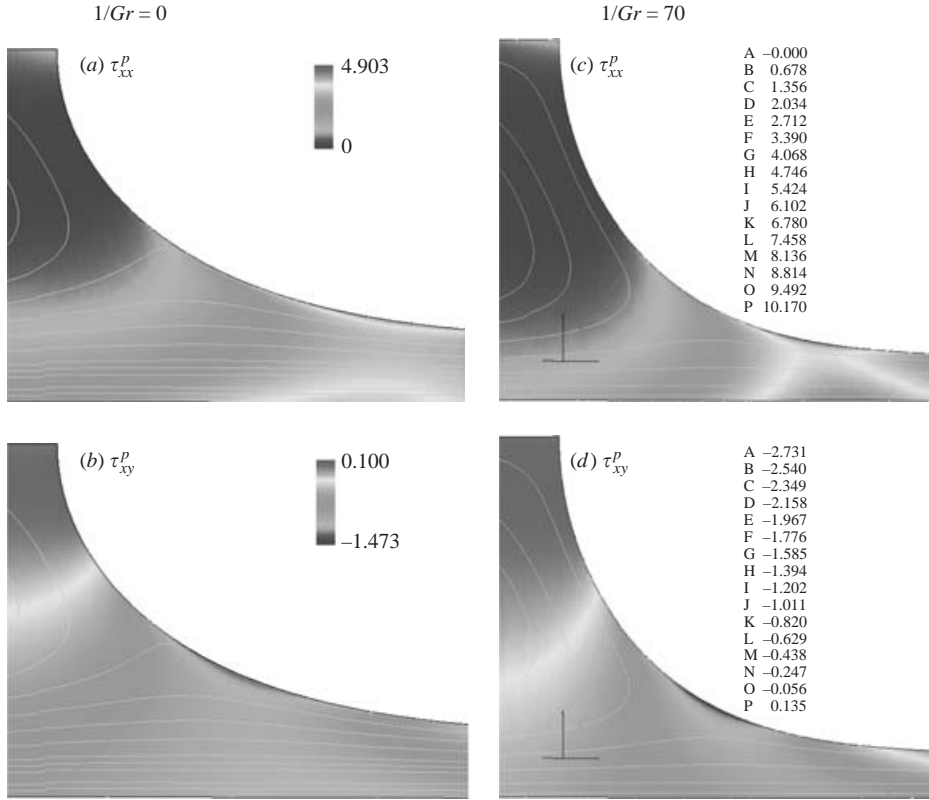


FIGURE 21. Numerical modelling of the gravity effects on polymeric stress distribution: ( $\tau_{xx}^p$  and  $\tau_{xy}^p$  at  $Ca=0.1$ ,  $Wi=0.3$ ,  $S=0.85$ , FENE-CR model).

and the values of the second invariant of the rate of strain tensor shown in figures 20(c) and 20(d) indicate an overall increase in the local shear/extension rates due to gravity forces. These rate increments are particularly pronounced in the vicinity of the two symmetric lateral stagnation lines located on the free surface. Figure 21 shows a direct comparison of the polymeric stresses (normal stress in the flow direction,  $\tau_{xx}^p$ , and shear stress,  $\tau_{xy}^p$ ) between flows in the surface-tension-dominated (figures 21a, b) and the gravity-dominated (figure 21c, d) regimes for  $Ca=0.1$  and  $Wi=0.3$ . Gravity is found to increase the maximum polymeric stresses, mainly localized in the capillary-transition region and in the proximity of the centre stagnation line, in the fluid by almost 50%. It is important to point out that while the polymeric stress accumulation in the surface-tension-dominated flow regime is concentrated in free surface stress boundary layers (figure 21a), in the gravity-dominated flow regime strong polymeric stress accumulation also occurs in the proximity of the confining walls (figure 21c). It has been shown by Lee *et al.* (2002) that the normal stress gradient induced by the formation of the stress boundary layer is responsible for the elastically driven film thickening. The magnification of the stresses in the capillary-transition region of the bubble front due to gravity could explain the increase in film thickening observed in our experiments compared to the measurements obtained by Huzyak & Koelling (1997), who conducted their experiments in the capillary flow regime. It is worth noting that the difference in flow geometry (planar versus axisymmetric) may have contributed to the differences in our measurements as well.

## 6. Summary

The DPIV technique is applied to study coating flow fields and it is found that in highly eccentric-cylinder forward-roll coating the number of stagnation lines is reduced to one (from three in nearly concentric flows) and its position is displaced far away from the meniscus region. Further investigation is needed to determine how this change in the flow field affects the stress distribution near the free surface and the stability of the interface.

We have discovered that in eccentric-cylinder forward-roll coating with gravity stabilization the elastic liquid free surface readily evolves into stable, two-dimensional sharp interfaces when the cylinders are almost concentric. It is found that when the gap width is small, the polymeric extensional stresses near the confining walls/cylinder surfaces can be strong enough to drive the geometric shape of these two-dimensional sharp interfaces away from the universal asymptotic relation of  $y = ax^{2/3}$  for cusps. Further investigation is needed to determine how the elastic stress fields vary with gap width in order to understand the formation mechanisms of these free surface singularities. A new form of stable bifurcation was also detected along the tip of these sharp interfaces formations.

Our film thickness measurements conducted under gravity stabilization showed a dramatic increase in coating thickness as a function of the flow  $Wi$ . While Huzyak & Koelling (1997) found that film thickening only occurred after the flow  $Wi$  exceeded unity in axisymmetric capillary flows, our measurements detected strong coating thickness increase even for values of  $Wi$  as low as 0.25.

In our computational work, a DEVSS finite element method coupled with pseudo-solid domain mapping technique was applied to analyse the free surface problems. The good qualitative agreement with our experimental observation of interfacial deformation for Newtonian liquids over a wide range of gravity and capillary numbers demonstrates the quality and robustness of our numerical scheme.

Our simulation results show that gravity dramatically increases the steepness of the stress boundary layer and the overall polymeric stress state in the capillary-transition region of the bubble front which may explain the strong film thickening observed in our experiments.

Our work provides an overview of viscoelastic interfacial phenomena in the gravity-dominated flow regime for eccentric cylinder coating. In addition to reproducing many of the viscoelastic effects previously reported, our experiments have uncovered a variety of new elasticity driven phenomena. In capturing the effects of gravity on the stress and flow field evolution in viscoelastic free surface flows our work may provide stronger physical grounds for performing future theoretical and computational analysis on this subject.

E. S. G. S. would like to thank the 3M Corporation and NSF for supporting this work through Grants 1DCH652 and 0090428, respectively. B. K. would like to thank NSF for supporting this work through Grant CTS-0089502. A. G. L. would also like to thank the National Science Foundation for support through their graduate research fellowship program. The authors are particularly grateful to Professor G. M. Homsy for his helpful comments and suggestions.

## REFERENCES

- ADACHI, K., SPIERS, R. P. & WILKINSON, W. L. 1978 Free coating of viscoelastic and viscoplastic fluids onto a vertical surface. *J. Non-Newtonian Fluid Mech.* **3**, 331–345.

- ALLEN, E. & BOGER, D. V. 1988 The influence of rheological properties on viscous fingering in enhanced oil recovery. *Xth Intl Congress on Rheology* (ed. P. H. T. Uiherr), ASR, Sydney, N.S.W., pp. 146–148.
- BAUMAN, T., SULLIVAN, T. & MIDDLEMAN, S. 1982 Ribbing instability in coating flows: Effect of polymer additives. *Chem. Engng Commun.* **14**, 35–46.
- BIRD, R. B., ARMSTRONG, R. C. & HASSAGER, O. 1987 *Dynamics of Polymeric Liquids*, 2nd Edn. Wiley.
- BOGER, D. V. & MACKAY, M. E. 1991 Continuum and molecular interpretation of ideal elastic fluids. *J. Non-Newtonian Fluid Mech.* **41**, 133–150.
- BONN, D., KELLAY, H., BRAUNLICH, M., BEN AMAR, M. & MEUNIER, J. 1995 Viscous fingering in complex fluids. *Physica A* **220**, 60–73.
- BRETHERTON, F. P. 1961 The motion of long bubbles in tubes. *J. Fluid Mech.* **10**, 166–188.
- CARVALHO, M. S. & KHESHGI, H. S. 2000 Low-flow limit in slot coating: theory and experiments. *Fluid Mech. Transport Phenom.* **46**, 1907–1917.
- CARVALHO, M. S. & SCRIVEN, L. E. 1999 Three-dimensional stability analysis of free surface flows: application to forward deformable roll coating. *J. Comput. Phys.* **151**, 534–562.
- CHAN, C. K. 2000 Surfactant wetting layer driven instability in a Hele-Shaw cell. *Physica A* **288**, 315–325.
- CHAN, C. K. & LIANG, N. Y. 1997 Observations of surfactant driven instability in a Hele-Shaw cell. *Phys. Rev. Lett.* **79**, 4381–4384.
- CHILCOTT, M. D. & RALLISON, J. M. 1988 Creeping flow of dilute polymer solutions past cylinders and spheres. *J. Non-Newtonian Fluid Mech.* **29**, 381–432.
- COYLE, D. J., MACOSKO, C. W. & SCRIVEN, L. E. 1990 Stability of symmetric film-splitting between counter-rotating cylinders. *J. Fluid Mech.* **216**, 437–458.
- DEBRUYN, J. R. & PAN, L. 1995 Delayed onset of ribbing instability due to finite-size effects. *Phys. Fluids* **7**, 2185–2190.
- DONTULA, P., PASQUALI, M., MACOSKO, C. W. & SCRIVEN, L. E. 1996 Viscoelastic effects in forward-roll coating flows. *Proc. XIIth Intl Congress on Rheology* (ed. A. Ait-kadi), Quebec City, Canada.
- DRIS, I. M. & SHAQFEH, E. S. G. 1995 On purely elastic instabilities in eccentric cylinder flows. *J. Non-Newtonian Fluid Mech.* **56**, 349–360.
- EDGAR, T. F. & HIMMELBLAU, D. M. 1988 *Optimization of Chemical Processes*. McGraw-Hill.
- ESMAIL, M. N. & HUMMEL, R. L. 1975 Nonlinear theory of coating onto a free surface. *AIChE J.* **21**, 958.
- FAIRBROTHER, F. & STUBBS, A. 1935 Studies in Electroendosmosis. Part IV. The bubble-tube method of measurements. *J. Chem. Sci.* **1**, 527.
- FERNANDO, R. H. & GLASS, J. E. 1988 Dynamic uniaxial extensional viscosity (DUEV) effects in roll application: II. Polymer blend studies. *J. Rheol.* **32**, 199–213.
- GIAVEDONI, M. D. & SAITA, F. A. 1997 The axisymmetric and plane cases of a gas phase steadily displacing a Newtonian liquid-A simultaneous solution of the governing equations. *Phys. Fluids* **8**, 2420–2428.
- GREENER, J., SULLIVAN, T., TURNER, B. & MIDDLEMAN, S. 1980 Ribbing instability of a two-roll coater: Newtonian fluids. *Chem. Engng Commun.* **5**, 73–83.
- GRILLET, A. M., LEE, A. G. & SHAQFEH, E. S. G. 1999 Observation of ribbing instabilities in elastic fluid flows with gravity stabilization. *J. Fluid Mech.* **399**, 49–83.
- GUENETTE, R. & FORTIN, M. 1995 A new mixed finite element method for computing viscoelastic flows. *J. Non-Newtonian Fluid Mech.* **60**, 27–52.
- GUO, H., HONG, D. C. & KURTZE, D. A. 1992 Surface-tension-driven nonlinear instability in viscous fingering. *Phys. Rev. Lett.* **69**, 1520–1523.
- GUTFINGER, C. & TALLMADGE, J. A. 1965 Films of non-Newtonian fluids adhering to flat plates. *AIChE J.* **11**, 403.
- HASSAGER, O. 1979 Negative wake behind bubbles in non-Newtonian liquids. *Nature* **279**, 402–403.
- HOMSY, G. M. 1987 Viscous fingering in porous media. *Annu. Rev. Fluid Mech.* **19**, 271–311.
- HUZYAK, P. C. & KOELLING, K. W. 1997 The penetration of a long bubble through a viscoelastic fluid in a tube. *J. Non-Newtonian Fluid Mech.* **71**, 73–88.
- JEONG, J.-T. & MOFFATT, H. K. 1992 Free-surface cusps associated with flow at low Reynolds number. *J. Fluid Mech.* **241**, 1–22.



- JOSEPH, D. D. & FENG, J. 1995 The negative wake in a second-order fluid. *J. Non-Newtonian Fluid Mech.* **57**, 313–320.
- JOSEPH, D. D., NELSON, J., RENARDY, M. & RENARDY, Y. 1991 Two-dimensional cusped interfaces. *J. Fluid Mech.* **223**, 383–409.
- LANDAU, L. D. & LEVICH, V. G. 1942 Dragging of a liquid by a moving plate. *Acta Physicochim. URSS* **17**, 42.
- LARSON, R. G. 1988 *Constitutive Equations for Polymer Melts and Solutions*. Butterworths.
- LARSON, R. G., SHAQFEH, E. S. G. & MULLER, S. J. 1990 A purely elastic instability in Taylor-Couette flow. *J. Fluid Mech.* **218**, 573–600.
- LEE, A. G. 2001 Viscoelastic effects on free-surface displacement flows: a computational and experimental study. PhD Thesis, Stanford University.
- LEE, A. G., SHAQFEH, E. S. G. & KHOMAMI, B. 2002 A study of viscoelastic free surface flows by the finite element method: Hele-Shaw and slot coating flows. *J. Non-Newtonian Fluid Mech.* **108**, 327–362.
- LIU, Y. J., LIAO, T. Y. & JOSEPH, D. D. 1995 A two-dimensional cusp at the trailing edge of an air bubble rising in a viscoelastic liquid. *J. Fluid Mech.* **304**, 321–342.
- LU, W. Q. & CHANG, H. C. 1988 An extension of the biharmonic boundary integral method to free surface flows in channels. *J. Comput. Phys.* **77**, 340.
- MAGDA, J. J. & LARSON, R. G. 1988 A transition occurring in ideal elastic liquids during shear flow. *J. Non-Newtonian Fluid Mech.* **30**, 1–19.
- MICHALLAND, S., RABAUD, M. & COUDER, Y. 1996 Instabilities of the upstream meniscus in directional viscous fingering. *J. Fluid Mech.* **312**, 125–148.
- MILL, C. C. & SOUTH, G. R. 1967 Formation of ribs on rotating rollers. *J. Fluid Mech.* **28**, 523–529.
- PASQUALI, M. & SCRIVEN, L. E. 2002 Free surface flows of polymer solutions with models based on conformation tensor. *J. Non-Newtonian Fluid Mech.* **108**, 363–409.
- PEARSON, J. R. A. 1959 The instability of uniform viscous flow under rollers and spreaders. *J. Fluid Mech.* **7**, 481–500.
- PITTS, E. & GREILLER, J. 1961 The flow of thin films between rollers. *J. Fluid Mech.* **11**, 33–50.
- POSLINSKI, A. J., OEHLER, P. R. & STOKES, V. K. 1995 Isothermal Gas-Assisted Displacement of Viscoplastic liquids in tubes. *Polym. Engng Sci.* **35**, 877–892.
- RABAUD, M., MICHALLAND, S. & COUDER, Y. 1990 Dynamical regimes of directional viscous fingering: Spatiotemporal chaos and wave propagation. *Phys. Rev. Lett.* **64**, 184–187.
- REINELT, D. A. & SAFFMAN, P. G. 1985 The penetration of a finger into a viscous fluid into a channel and tube. *SIAM J. Sci. Stat. Comput.* **6**, 542.
- RO, J. S. & HOMS, G. M. 1995 Viscoelastic free surface flows: thin film hydrodynamics of Hele-Shaw and dip coating flows. *J. Non-Newtonian Fluid Mech.* **57**, 203–225.
- RUSCHAK, K. J. 1983 A three dimensional linear stability analysis for two-dimensional free boundary flows by the finite element method. *Comput. Fluids* **11**, 391.
- RUSCHAK, K. J. 1985 Coating flows. *Annu. Rev. Fluid Mech.* **17**, 65–89.
- SAFFMAN, P. G. & TAYLOR, G. 1958 The penetration of a fluid into a porous medium or Hele-Shaw cell containing a more viscous liquid. *Proc. R. Soc. Lond. A* **245**, 312–329.
- SOULES, D. A., FERNANDO, R. H. & GLASS, J. E. 1988 Dynamic uniaxial extensional viscosity(DUEV) effects in roll application: I. Rib and web growth in commercial coatings. *J. Rheol.* **32**, 181–198.
- SPIERS, R. P., SUBBARAMAN, C. V. & WILKINSON, W. L. 1975 Free coating of non-Newtonian liquids onto a vertical surface. *Chem. Engng Sci.* **30**, 379.
- SULLIVAN, T. M. & MIDDLEMAN, S. 1979 Roll coating in the presence of a fixed constraining boundary. *Chem. Engng Commun.* **3**, 469–482.
- TAYLOR, G. I. 1960 Deposition of a viscous fluid on the wall of a tube. *J. Fluid Mech.* **10**, 161–165.
- THARMALINGAM, S. & WILKINSON, W. L. 1978 The coating of Newtonian liquids onto a rotating roll. *Chem. Engng Sci.* **33**, 1481–1487.
- WHITE, D. A. & TALLMADGE, J. A. 1965 Theory of drag out of liquids on flat plates. *Chem. Engng Sci.* **20**, 33–37.